

Competing Annulene and Radialene Structures in a Single Anti-Aromatic Molecule Studied by High-Resolution Atomic Force Microscopy

Shigeki Kawai,^{*,†,‡,§} Keisuke Takahashi,[§] Shingo Ito,^{*,§,||} Rémy Pawlak,^{||} Tobias Meier,^{||} Peter Spijker,^{⊥,¶} Filippo Federici Canova,[¶] John Tracey,[⊥] Kyoko Nozaki,^{§,||} Adam S. Foster,^{*,⊥,△} and Ernst Meyer^{||}

[†]International Center for Materials Nanoarchitectonics, National Institute for Materials Science, 1-1, Namiki, Tsukuba, Ibaraki 305-0044, Japan

[‡]PESTO, Japan Science and Technology Agency, 4-1-8, Honcho, Kawaguchi, Saitama 332-0012, Japan

[§]Department of Chemistry and Biotechnology, Graduate School of Engineering, The University of Tokyo, 7-3-1 Hongo, Bunkyo-ku, Tokyo 113-8656, Japan

^{||}Department of Physics, University of Basel, Klingelbergstrasse 82, CH-4056 Basel, Switzerland

[⊥]COMP, Department of Applied Physics, Aalto University, P.O. Box 11100, FI-00076 Aalto, Finland

[¶]Netherlands Organisation for Scientific Research, Domain Science, P.O. Box 3021, 3527 JP, Utrecht, The Netherlands

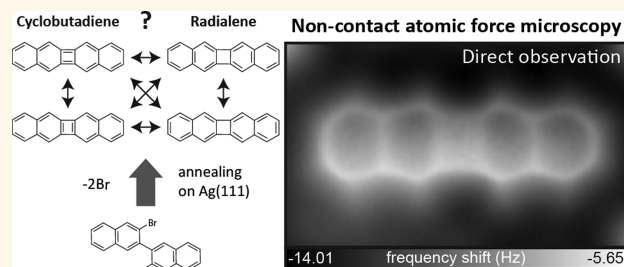
[¶]Nanolayers Research Computing LTD, 15 Southgrove Road, Sheffield, United Kingdom, S10 2NP

[△]Division of Electrical Engineering and Computer Science, Kanazawa University, Kanazawa 920-1192, Japan

Supporting Information

ABSTRACT: According to Hückel theory, an anti-aromatic molecule possessing $(4n)\pi$ -electrons becomes unstable. Although the stabilization has been demonstrated by radialene-type structures—fusing aromatic rings to anti-aromatic rings—in solution, such molecules have never been studied at a single molecular level. Here, we synthesize a cyclobutadiene derivative, dibenzo[*b,h*]biphenylene, by an on-surface intramolecular reaction. With a combination of high-resolution atomic force microscopy and density functional theory calculations, we found that a radialene structure significantly reduces the anti-aromaticity of the cyclobutadiene core, extracting π -electrons, while the small four-membered cyclic structure keeps a high density of the total charge.

KEYWORDS: on-surface chemical reaction, anti-aromaticity, radialene, chemical structure, atomic force microscopy, density functional theory calculation



The Hückel rule dictates that cyclic molecules with $(4n + 2)\pi$ electrons (where n is an integer), called aromatic compounds, are stabilized by efficient delocalization of π -electrons. The best-known example of such a molecule is benzene with $n = 1$. In the case of molecules with $(4n)\pi$ electrons, on the other hand, the cyclic delocalization of π electrons is destabilizing, making the molecule more unstable than aromatic and nonaromatic congeners; this characteristic is classified as anti-aromaticity. Cyclobutadiene, with 4π electrons ($n = 1$), is known to be highly unstable not only due to its anti-aromaticity but also because of the ring strain imposed by a four-membered cyclic structure. This forces departure of the

C–C–C angles to 90° from the preferred 120° (Figure 1a).^{1–3} Therefore, the synthesis and direct structural analysis of simple and small cyclobutadiene molecules has been rather challenging, requiring kinetic stabilization by bulky substituents (Figure 1b)^{4–6} or by confinement into crystals.⁷ An alternate, but efficient, method to stabilize cyclobutadiene derivatives is by fusing aromatic rings to a four-membered backbone. Biphenylene, in which two benzene rings are fused to the

Received: April 30, 2017

Accepted: July 15, 2017

Published: July 16, 2017

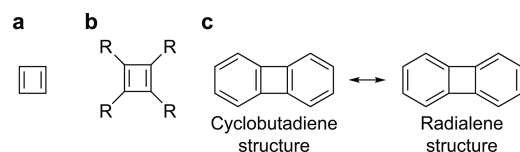


Figure 1. (a) Cyclobutadiene, (b) tetrasubstituted cyclobutadiene, and (c) biphenylene.

cyclobutadiene core, is quite stable both chemically and thermally (Figure 1c).⁸ This may be partly due to stabilization imparted by a radialene structure, which is a cyclic structure containing cross-conjugated exocyclic double bonds, rather than the corresponding cyclobutadiene structure. Although the structures of biphenylene and related compounds have been confirmed by X-ray diffraction^{9–12} and electron diffraction¹³ analyses, such reciprocal space measurements are potentially influenced by a dynamic and static disorder of molecules in crystals.^{3,14,15} Therefore, it is of importance to investigate the radialene structure of cyclobutadiene derivatives at a single molecular level.

State-of-the-art atomic force microscopy (AFM) has become an important technique in a field of on-surface chemistry, since the functionalized tip with a small carbon monoxide (CO) molecule allows us to observe the inner structures of single molecules on surfaces.¹⁶ This direct observation has been used to investigate new molecules,¹⁷ including asphaltenes,¹⁸ as well as on-surface chemical reactions.^{19,20} Even the bond order can be investigated by measuring the apparent bond length.²¹ Furthermore, together with local probe-induced dehydrogenation or dehalogenation, high-resolution AFM has been used for identifying the structures of arynes²² and triangulene,²³ as well as for tracking the reversible Bergman cyclization.²⁴ Therefore, AFM is a logical tool to address a radialene structure in single biphenylene derivatives via direct observation.

Here, using the AFM technique with the CO functionalized tip we study the structure and anti-aromaticity of a single dibenzo[*b,h*]biphenylene,^{25–31} which was synthesized *in situ* by on-surface intramolecular reactions. The measured bond lengths in the naphthalene moieties connected to the cyclobutadiene core provide insight into competing annulene and radialene structures in a single compound. We found that anti-aromaticity is significantly reduced, yet the total charge density in the small cyclobutadiene core is strengthened by the large stress of the carbon–carbon bond, inducing stronger short-range repulsion. However, at a large tip–sample separation, the reduced total charge of the radialene structure leads to a weaker tip–sample attractive interaction. Our density functional theory (DFT) calculations show an important role in the dissociated bromine atoms for the condensation of molecules. Furthermore, the order of the calculated bond order and the behavior of the total charge support the experimental results.

RESULTS AND DISCUSSION

On-Surface Ullman-Type Intermolecular Reaction.

Ullmann-type chemical reactions have recently been employed to synthesize conjugated polymers from hydrocarbons on metal surfaces.^{32–34} In such precursors, two halogen (Br and I) atoms are substituted at the both sides and hence the intermolecular reaction takes place by annealing. We took a similar strategy to form the intramolecular bond by employing 3,3'-dibromo-2,2'-binaphthalene (Figure 2a), in which two naphthalene moieties

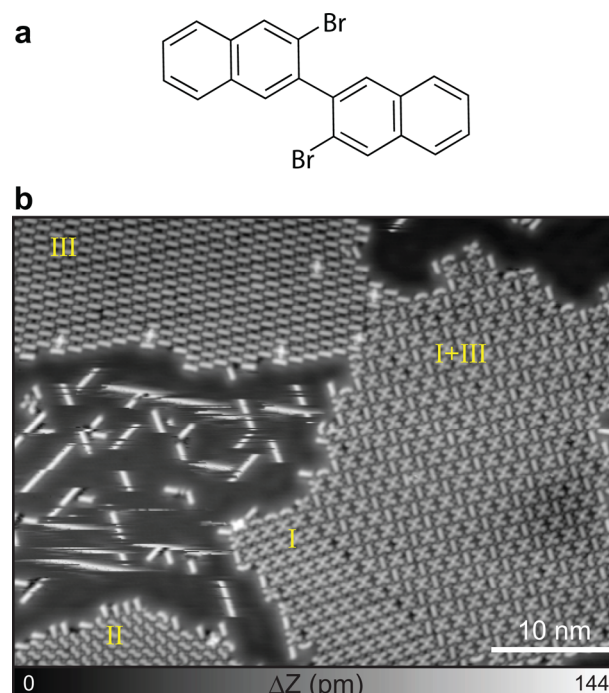


Figure 2. (a) Schematic drawing of 3,3'-dibromo-2,2'-binaphthalene. (b) Scanning tunneling microscopy (STM) topography of the compound synthesized on Ag(111) at 406 K. Measurement parameters: Bias voltage $V_{\text{tip}} = -200$ mV and tunneling current $I = 0.8$ pA.

are connected to each other with a single bond. By connecting position 3 and 3', dibenzo[*b,h*]biphenylene can be synthesized. The precursor was deposited on Ag(111) at 366 K while the temperature of the substrate was kept at room temperature. Subsequently, the sample was annealed at 406 K to induce the on-surface chemical reaction, which is assisted by the catalytic properties of the surface.³⁵ Figure 2b shows an overview of the STM topography taken with a CO functionalized tip. We found three different kinds of compounds on the surface, labeled as I, II, and III. Similar to previous studies,^{36,37} the synthesized compounds were condensed via the halogen atoms dissociated from the precursors. The important role of the dissociated halogen atoms in the stabilization of the molecular film can be seen by the noisy lines in the left-hand side in Figure 2b, where isolated molecules were accidentally moved by the scanning probe even with a large tip–sample separation (0.8 pA and -200 mV). A detailed condensation mechanism will be discussed in the section of theoretical calculations. Note that we also see evidence of co-condensation of molecular types. On the right-hand side in Figure 2b, the co-condensation of molecule I and III is seen, while molecule I and II are shown in Figure S1. In all cases, the structures including the halogen atoms were highly ordered.

Figure 3a–c show closeup views of STM topographies of molecule I, II, and III, in which butterfly-, 'S'-, and linear-shaped molecules can be seen, respectively. From the observed molecular size, we can immediately conclude that molecule I is composed of two precursors. The bright spot at the center of molecule I corresponds to a Ag atom, as indicated by a red arrow in the inset of Figure 3a, which is consistent with the previous works on organometallic compounds.^{38,39} Smaller bright spots indicated by yellow arrows likely correspond to the dissociated Br atoms. Two other compounds are composed of

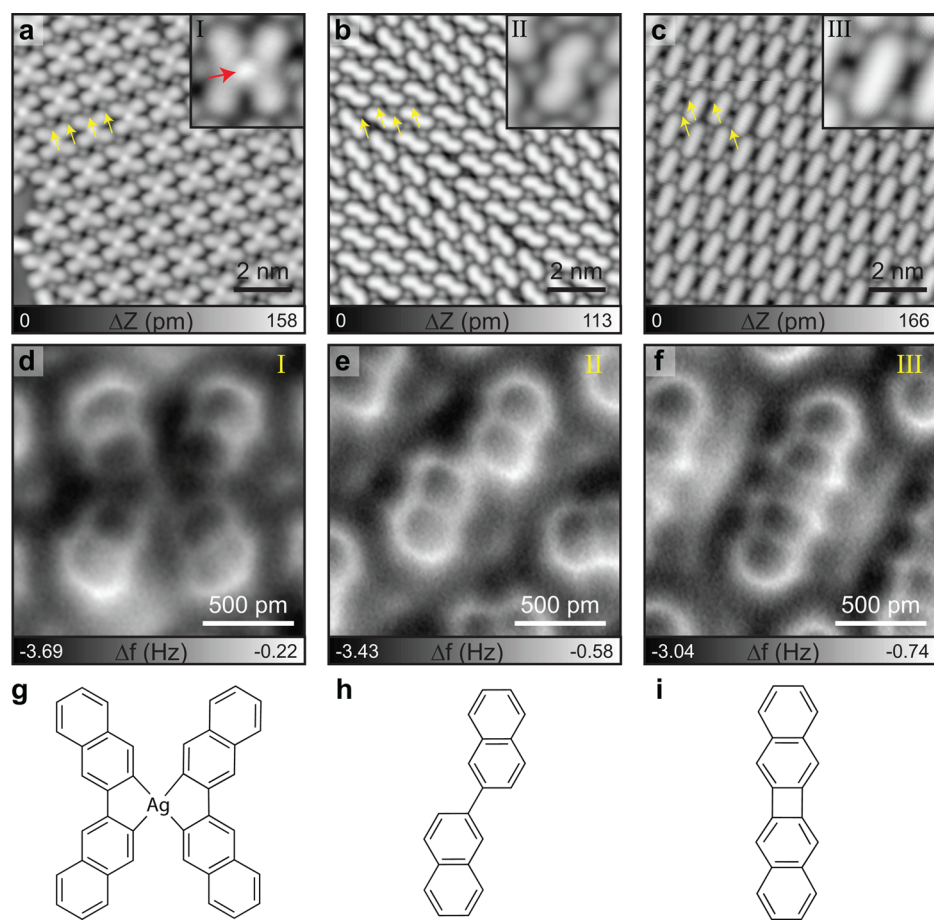


Figure 3. (a–c) STM topographies of the compounds synthesized on Ag(111) at 440 K. Insets show closeup views. (d–f) Corresponding atomic force microscopy (AFM) images, obtained with a CO functionalized tip. (g–i) Chemical structures of the organometallic compound, 2,2'-binaphthalene, and dibenzo[*b,h*]biphenylene. Measurement parameters: $V_{\text{tip}} = -200$ mV and $I = 0.8$ pA for STM measurements in (a–c). $V_{\text{tip}} = 0$ mV and oscillation amplitude $A = 60$ pm for AFM measurements in (d–f).

single precursors (Figure 3b and c), yet the shapes are different, as seen in the insets. In order to investigate the molecular structures, we switched to AFM and observed the products with a CO functionalized tip at a constant height. Figure 3d–f show the corresponding high-resolution AFM images and chemical structures (Figure 3g–i). The organometallic compound (molecule I) appears with a dark contrast at the center, and the four termini are brighter. Molecule II is 2,2'-binaphthalene, so two bromines in the precursor molecule were replaced by two hydrogen atoms.

Interestingly, two radicals were formed by cleaving two sets of the C–Br σ bonds in each molecule via annealing and were immediately hydrogenated before the precursors conjugated to each other or themselves. In this reaction, no hydrogen atoms were released from the precursor, so that hydrogen atoms were definitely supplied from the UHV environment or the Ag substrate. Note that hydrogen atoms from the tungsten filament located at the backside of the sample plate for heating may also be the candidate, yet the pressure during annealing at 406 K never exceeded 1×10^{-9} mbar. Nevertheless, stray hydrogen atoms were abundant and generally play an important role in any Ullmann-type on-surface reaction in vacuum. The hydrogenation of the radicals was not perfect, so that some of the precursors were self-terminated as initially designed. Molecule III is the target compound, which is dibenzo[*b,h*]biphenylene (Figure 3f and i).⁴⁰ Note that the yield of each

compound can be changed by the annealing temperature. Annealing at a lower temperature of 356 K mainly induced the formation of molecule I (see Supporting Information Figure S2). Furthermore, by annealing at 406 K, a signature of transformation to molecule II from the organometallic compound was seen (Figure S1). Therefore, the organometallic compound (Figure 3d) is the intermediate. Depositing the precursor on the substrate kept at 440 K selectively produced only molecule III (see Supporting Information Figure S3). It may relate to the fact that the ratio of hydrogenation of the radical and self-conjugation drops at a higher temperature, or molecule II desorbs from the surface due to a lower binding energy, compared with molecule III.

Structural Analysis of Dibenzobiphenylene. Here, we focus on the structure of dibenzo[*b,h*]biphenylene (Figure 4a). The molecule is planar and symmetric, having two naphthalene moieties, connected with the cyclobutadiene core. The four centers of both naphthalene moieties are observed equivalently. In contrast, the cyclobutadiene core appears brighter (more positive frequency shift) than the naphthalene moieties with a certain tip–sample separation. It can be related to either the anti-aromaticity, the size of cyclic carbon, or the strong distortion of C–C–C bond. The observed cyclobutadiene core looks like the rectangular D_{2h} structure. According to the pioneering work on bond order analysis with AFM,²¹ a higher (lower) bond order appears shorter

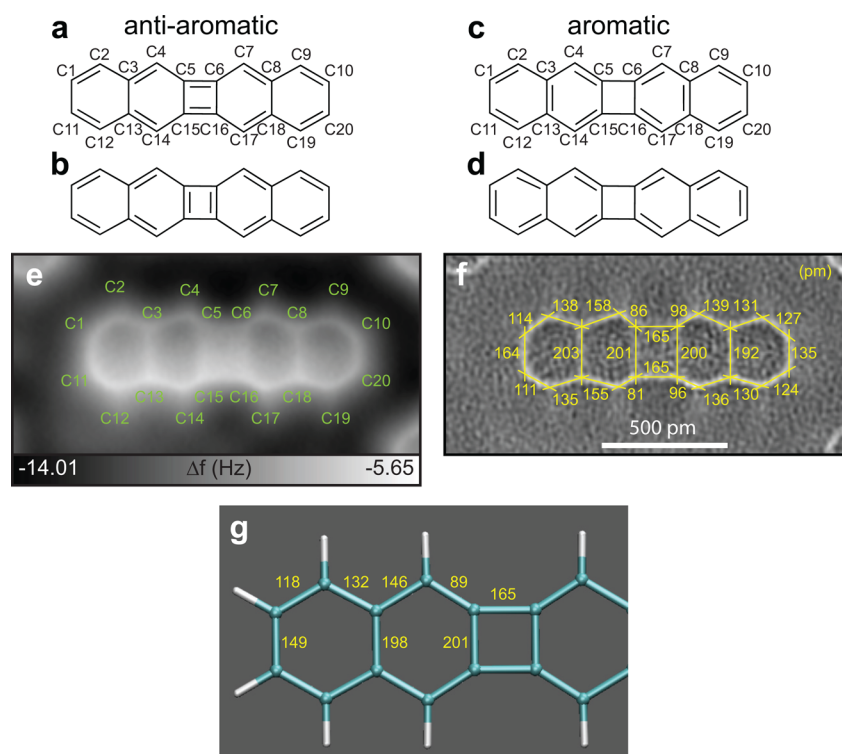


Figure 4. (a–d) Schematic drawing of dibenzo[*b,h*]biphenylene. (e) High-resolution AFM image, obtained with a CO functionalized tip. (f) Corresponding Laplace filtered image for a better view of the bonds. The numbers indicated the measured bond lengths. (g) Mean values of the bond lengths taken over equivalent bonds.

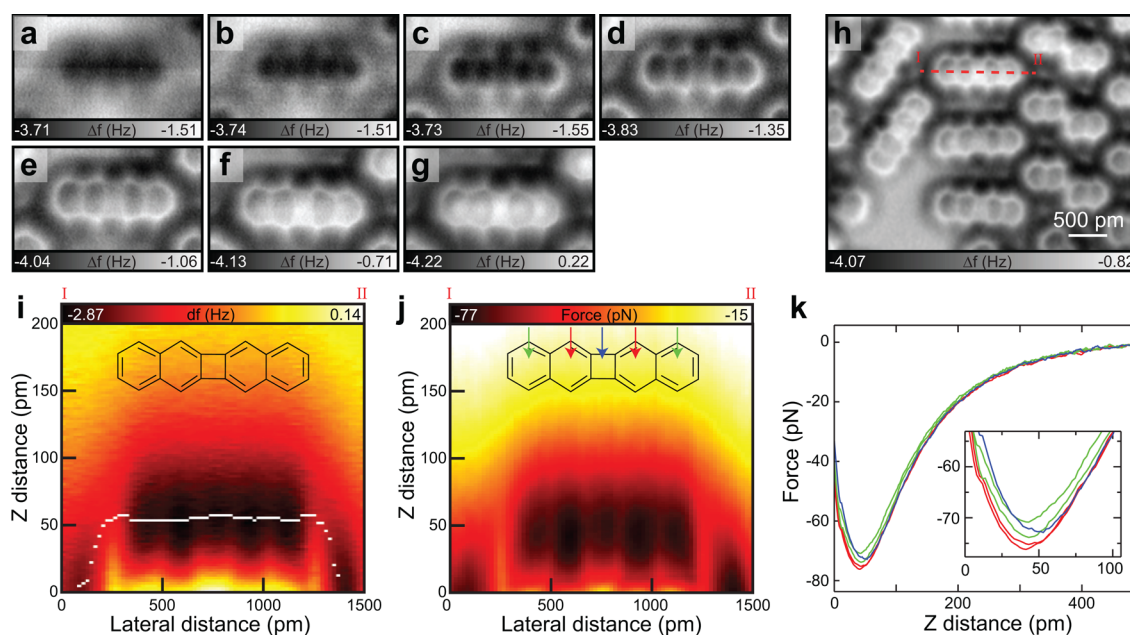


Figure 5. (a–g) A series of AFM images, taken at different tip–sample distances. The distance step between images is 20 pm, with (a) the furthest from the sample. (h) High-resolution AFM image. (i) Two-dimensional frequency shift map taken along the dashed line in h. White dots indicate the Z position of the most negative frequency shift in each Z– Δf curve. (j) Extracted force map. (k) Force curves at the centers of the cyclic carbons. The positions were indicated in (j). Measurement parameters: $V_{\text{tip}} = 0$ mV and $A = 60$ pm.

(longer). The tiny difference of the bond length is significantly amplified by the tilt effect of the CO tip. Therefore, at first glance, one might readily conclude that anti-aromaticity is the leading candidate to explain the image contrast. However, such bond length extension can also be seen in the naphthalene moieties, which are supposed to be mostly aromatic. Thus, the

tilt effect of the CO tip is responsible for the apparent extension of the cyclic carbons. While the CO tip ensures imaging of inner structures of molecules, the low lateral stiffness is strongly affected by the asymmetric force field.⁴¹ Especially, when a molecule is rectangular, the lateral force gradient along the short molecular axis is steeper than that along the longitudinal

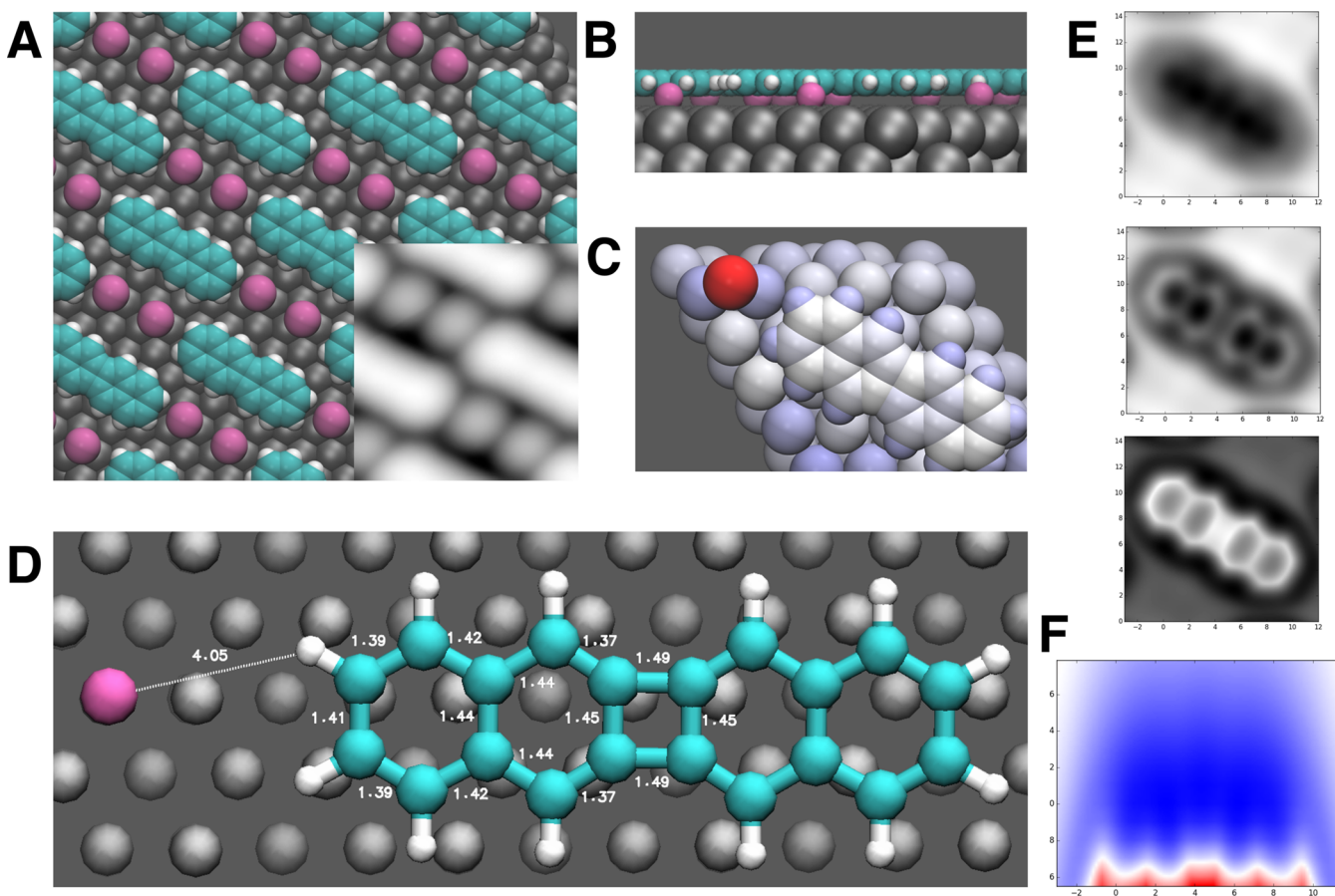


Figure 6. Calculated structure of condensed dibenzo[*b,h*]biphenylene molecular structure on the [111] silver surface from (a) top and (b) side. Atoms are colored as follows: C (Cyan); H (white); Br (mauve); Ag (silver). The inset in (a) shows an example constant current simulated STM image of the system. (c) Plot of charge of adsorbed system, where red is negative and blue is positive (plotted range $-0.45:0.30$). (d) Zoom into one molecule to show bond lengths in the calculated structure. (e) Simulated AFM images of an isolated molecule with decreasing tip–surface distance from top to bottom. (f) Simulated force map taken along the center-line of the molecule. Here white is zero interaction, blue is attraction, and red is repulsion.

axis. In this way, the molecule appears to be extended in the direction of the short axis as seen in Figure 3f. This feature was observed even in the first observation with pentacene¹⁶ (for a better comparison, see Supporting Information Figure S4). Therefore, the direct analysis of the bond order only at the small cyclobutadiene core is not trivial.

Since the aromaticity and anti-aromaticity at the core affects those of connected naphthalene moieties, these can indirectly be investigated via bond length analysis of the naphthalene moiety. In the case of molecule III, the lateral force field along the same axis would be almost constant, leading to the same magnitude of tip deflection. Note that bonds at both edges usually appear longer than those at the centers due to a steeper lateral force gradient toward the center of the molecule. In contrast to the small cyclobutadiene core, analyses of the bond length at the naphthalene moiety thus become valid. Several contributing structures are drawn in Figure 4a–d, in which carbon atoms are labeled as C1–C20. Figure 4e shows a high-resolution AFM image, while, in Figure 4f, to enhance the bond features, a Laplace filter was applied.²¹ To cancel the effect of the anisotropic tilt of the CO molecule, we took mean values over the equivalent bonds in molecule III (Figure 4g). We then investigated the bond order along the longitudinal axis. If the anti-aromaticity remains at the cyclobutadiene core, C3–C4 and C4–C5 should be double and single bonds, respectively

(Figure 4a and b). However, the observed bond length of C3–C4 (146 pm) is much longer than C4–C5 (89 pm), so the bond order of C3–C4 is lower than C4–C5. Therefore, the anti-aromaticity of cyclobutadiene core, in the so-called radialene structure (Figures 4e and f), is drastically reduced by the fused naphthalene moieties. Nevertheless, the unusual short length of the C4–C5 bond may also relate to a local geometrical compensation caused by the CO tip deflection since the C5–C6 bond appears significantly longer. Next, we investigated the weight of two aromatic resonance structures via comparing the bond lengths among C1–C2, C2–C3, and C3–C4. The longest bond is C3–C4 (146 pm), followed in order by C2–C3 (132 pm) and C1–C2 (118 pm). If the naphthalene moiety keeps its aromaticity, this condition cannot be satisfied with only two radialene structures, since the C1–C2 bond should be the same as C2–C3. Note that the apparent C1–C2 bond length is elongated by the edge effect. To satisfy this condition, a low, but finite weight of annulene structures should exist, while the majority weight comes from the two radialene structures. Hence, the radialene structure is not completely dominant and can be considered a so-called partial radialene. Note that the bond length analysis requires clear bond features in the image,²¹ which can be obtained only in a small range of the *Z* distance. We see no significant systematic change of the measured bond lengths as a function of *Z*.

Quantitative Force Measurement of the π System.

Figure 5a–g shows a series of AFM images, taken at different tip–sample Z distances. The step of the Z distance was 20 pm. A strong contrast transition of the AFM images at the cyclobutadiene core is seen. At large tip–sample separations, the contrast at the cyclobutadiene is blurred, as if the two naphthalene moieties are disconnected (Figure 5c). In order to investigate the tip–sample interaction quantitatively, a series of Z distance dependent measurements was taken along the longitudinal molecular axis (Figure 5h). Figure 5i shows the two-dimensional frequency shift map. Note that although nonsite dependent long-range contributions were subtracted, the attractive van der Waals interaction between tip and molecule modulates the force field, such that a dark halo appears around the molecule (Figure 5h). Consequently, the center of molecule has the greatest attractive force background. The center core looks slightly protruded due to the strongly increased frequency shift at close distances. To investigate the corrugation across a single molecule, we took the most negative frequency shift points, which can indicate a variation of the local adsorption height.⁴² The center of the cyclobutadiene core is shifted farther from the surface than those of the naphthalene moieties by about 6 pm. In order to get a better physical quantity, the interaction force was extracted via the frequency shift map with a numerical algorithm (Figure 5j).⁴³ We found that the magnitude of the attractive force at the cyclobutadiene core is lower than that at the centers of the benzenes (Figure 5k), while the repulsive force rapidly grows in a similar fashion.

Density Functional Calculations. In order to gain more insight into the nature of the dibenzo[*b,h*]biphenylene molecular structure on the Ag (111) surface, we performed a series of density functional theory (DFT) calculations. Initially we considered the adsorption of isolated molecules on the surface and found that they adsorb with an energy gain of 1.88 eV, and an adsorption height at the cyclobutadiene core of 310 pm (with the edges at about 295 pm). There is minimal charge transfer with the surface, and the bond lengths are almost identical to the molecule in vacuum—there is a clear upward shift of the molecule center of about 15 pm, which is larger than the value extracted via the experimental data (see Figure 5i). Although small, CO-AFM imaging is highly sensitive to these differences³⁴ and the associated simulated images differ significantly from the experimental images (see Supporting Information Figure S5b).

The calculations were then repeated in the presence of cleaved bromines in the initial geometry suggested by STM (see Figure 3c). Electron transfer from the surface to the bromines (see Supporting Information Figure S6) results in a clear charge on them (estimated at $-0.5e$) and a smaller positive charge on the neighboring Ag atoms (see Figure 6c). This leads to a small, but non-negligible, electrostatic interaction between the negative Br ions and positive molecular hydrogens, as well as increased polarization effects, overall providing a gain of 0.34 eV compared to the isolated molecules on Ag (based on a formation energy comparison of equivalent components). The interaction also flattens the molecule, with a vertical variation of less than 3 pm (see Figure 6b), and simulated AFM images are now much closer to that seen experimentally (see Figure 6e); in particular, the clear variation in contrast across the molecule in Figure S5 at smaller tip–surface distances is not present in Figure 6e. The molecule–substrate separation becomes larger on average (to about 312 pm), but the molecule remains effectively identical to the

vacuum structure. The introduction of bromine also means that simulated STM images show very good agreement with experiment (see Figure 6a), and we also produce a simulated force map (Figure 6f) that shows all the main features seen in experiments (Figure 5j). Note that the adsorption energy of a single bromine atom is about 4 eV, while the dissociation energy of the dimer is about 2 eV, so it is extremely unfavorable to desorb bromine. Also, despite the very fast diffusion of bromine on metal surfaces,⁴⁴ its negative charge prevents the formation of dimers on the surface.

If we consider the development of AFM contrast shown in Figure 5a–g and Figure 6e, the gradual appearance of the cyclobutadiene core is related to the nature of charge and charge density of the system. At longer ranges, the weakly charged atoms (charges ± 0.05) of the molecule show a weak contrast, and the background dominates; repulsive interactions are minimal. As the tip approaches, the total charge density in the C–C bond is responsible for the strength of the short-range repulsion and the concentration of charge density at the core due to the proximity of the four carbon atoms means the short-range repulsion rapidly grows at a small separation. Moving even closer, the centers of cyclic carbons at the naphthalene moieties also started to be filled by the bright contrast (Figure 5g), again relating to the short-range repulsion.²¹

The lack of significant charge transfer between the molecule and metal substrate allows us to investigate the competing annulene and radialene structures. Figure 6d shows the calculated geometry of the molecule. Small, but significant variations of the bond length can be seen across the molecule. In Table 1, the measured bond lengths in the experiments and

Table 1. Bond Order Analysis *via* the Bond Lengths

Bond	AFM measurement (pm)	DFT calculation (pm)	Pauling bond order
C1–C2	118	139	1.64
C2–C3	132	142	1.50
C3–C4	146	144	1.42
C4–C5	89	137	1.73
C5–C6	165	149	1.23
C1–C11	149	141	1.55
C3–C13	198	145	1.38
C5–C15	201	145	1.38

the calculations are listed. Due to the amplification of the bond order difference by the deflection of the CO tip, the absolute value deviates, yet the order of the lengths along the longitudinal molecular axis agrees well (see Supporting Information Figure S7). Nevertheless, to obtain more chemical quantities, we calculated the bond orders (also shown in Table 1) with the bond lengths obtained in the DFT calculations. The relationship between the Pauling bond order and the bond length is described as

$$n_x = n_0 \exp\left(\frac{r_0 - r_x}{c}\right) \quad (1)$$

where n_x is the bond order, r_x the bond length, n_0 the bond order of the reference, and r_0 the bond length of the reference. The constant $c = 0.353$ was taken from ref 45. Since the tetragonal core of dibenzo[*b,h*]biphenylene contains strong ring strain, the absolute bond orders may have uncertainties, but the relative values should be valid. The Pauling bond orders in the naphthalene moiety significantly vary around 1.601,

indicating that all bonds are between single and double bonds. Particularly, C4–C5 has more double bond character due to the fused cyclobutadiene core, as shown in Figure 4c and d. However, since the radialene structure is not perfect, the corresponding Pauling bond order is much lower than 2. In this way, the calculated Pauling bond shows evidence that the aromaticity of the naphthalene moiety is modulated by the radialene structure.

CONCLUSION

In summary, we reported competing annulene and radialene structures in a single cyclobutadiene derivative. High-resolution atomic force microscopy with a CO functionalized tip allowed investigation of the deviation of the π electron system *via* bond length comparison. While the anisotropic force field in the rectangular shape at the core prevented a direct investigation of the anti-aromaticity in the cyclobutadiene, the fused naphthalene core gave insights into the radialene structure indirectly. We found that the radialene structure significantly reduces the anti-aromaticity in the cyclobutadiene core yet is not perfect. DFT calculations emphasized the role of cleaved bromines in the resulting structure and demonstrated that charge transfer from the surface did not play a significant role in the electronic structure of the adsorbed molecules on the surface. This then justified the use and interpretation of AFM bond order analysis and highlighted its potential in future studies of the nature of the π electron in cyclic carbon compounds.

METHODS

AFM Measurements. All measurements were performed with a commercially available Omicron low temperature scanning tunneling microscopy (STM)/atomic force microscopy (AFM) system, operating in ultrahigh vacuum at 4.8 K. We used a tuning fork with a chemically etched tungsten tip as a force sensor.⁴⁶ The resonance frequency and the mechanical quality factor are 23145.6 Hz and 5033, respectively. The high stiffness of 1800 N/m realizes a stable operation with a small amplitude of 60 pm.⁴⁷ The frequency shift, caused by the tip–sample interaction, was detected with a commercially available digital phase-locked loop (Nanonis: OC-4 and Zurich Instruments: HF2-LI and HF2-PLL).⁴⁸ For the STM measurement, the bias voltage was applied to the tip while the sample was electronically grounded. The tip apex was *ex situ* sharpened by milling with a focused ion beam. The tip radius was less than 10 nm. A clean silver tip was *in situ* formed by indenting to the Ag sample surface and applying a pulse bias voltage between tip and sample several times. For AFM, the tip apex was terminated with a CO molecule, which was picked up from the surface.⁴⁹ Clean Ag(111) surfaces were *in situ* prepared by repeated cycles of standard Ar⁺ sputtering (3×10^{-6} mbar, 1000 eV, and 15 min) and annealing at 740 K. In this experiment, 3,3'-dibromo-2,2'-binaphthalene molecules were deposited on the surface from crucibles of a Knudsen cell, heated at 366 K. The temperature of the substrate was kept at room temperature. Two-dimensional frequency shift mapping was performed by a series of Z distance measurements of the frequency shift. Measured images were analyzed using the WSxM software.⁵⁰

Theoretical Calculations. All first-principles calculations in this work were performed using the periodic plane-wave basis VASP code^{51,52} implementing the spin-polarized density functional theory (DFT). To accurately include van der Waals interactions in this system we used the optB86B+vdW-DF functional,^{53–55} selected based on previous work showing that it provides a sufficiently accurate description for all subsystems involved in the measurement. Projected augmented wave (PAW) potentials were used to describe the core electrons,⁵⁶ with a kinetic energy cutoff of 550 eV (with PREC = accurate). Systematic *k*-point convergence was checked for all systems, with sampling chosen according to system size and a mesh of $3 \times 3 \times$

1 being used for the final production runs. This approach converged the total energy of all the systems to the order of meV. The properties of the bulk and surface of Ag and the isolated molecular structure were carefully checked within this methodology, and excellent agreement was achieved with experiments. For calculations of the isolated molecule, a surface slab of $6 \times 6 \times 5$ in terms of the Ag unit cell was used, with a vacuum gap of at least 1.5 nm. This was reduced to $5 \times 5 \times 5$ to match the dimensions of the condensed phase seen in experiments. All adsorption energies are calculated by subtracting the individual components of the system, in the same unit cell, from the total energy of the final system. Bader charge analysis was used to estimate charge transfer in the simulations.⁵⁷ We also calculated the isolated molecular structure using hybrid functional B3LYP,^{58,59} and the adsorbed molecule–surface structure using vdW functionals D3⁶⁰ and TS.⁶¹ We observed no significant differences in the structure compared to optB86B.

For calculated AFM images we used the model developed by Hapala et al.⁶² The best agreement with experiment was found with a tip lateral spring constant of about 0.5 N/m, similar to values reported in previous studies.⁶² The molecular structure was taken from DFT simulations of the adsorbed molecule, and the electrostatic potential was extracted from the Hartree potential;⁶³ we also used a quadrupole dz² tip model,⁶⁴ with an effective charge of -0.2 , which proved critical in getting excellent agreement with experiment. All other parameters are the same as intended by Hapala et al., and the simulated AFM scan is performed at a resolution of 2.5 pm (in all directions), with a force tolerance criterion of 4×10^{-6} eVÅ⁻¹. The 3D force field is subsequently converted into a frequency shift image using the experimental parameters.

ASSOCIATED CONTENT

Supporting Information

The Supporting Information is available free of charge on the ACS Publications website at DOI: 10.1021/acsnano.7b02973.

Coexisting of compound I and II, self-assembly of the organometallic compound, deposition on a hot Ag(111) at 440 K, influence of the radialene structure, calculation of a single dibenzo[*b,h*]biphenylene molecule, induced differential charge density, and measured bond length as a function of Pauling bond order are discussed. (PDF)

AUTHOR INFORMATION

Corresponding Authors

*Kawai.shigeki@nims.go.jp (S.K.).

*ito_shingo@chembio.t.u-tokyo.ac.jp (S.I.).

*adam.foster@aalto.fi (A.S.F.).

ORCID

Shigeki Kawai: 0000-0003-2128-0120

Shingo Ito: 0000-0003-1776-4608

Rémy Pawlak: 0000-0001-8295-7241

Tobias Meier: 0000-0003-0606-5131

Kyoko Nozaki: 0000-0002-0321-5299

Adam S. Foster: 0000-0001-5371-5905

Notes

The authors declare no competing financial interest.

ACKNOWLEDGMENTS

This work was supported in part by the Japan Science and Technology Agency (JST) 'Precursory Research for Embryonic Science and Technology (PRESTO)' for a project of 'Molecular technology and creation of new functions', by Japan Society for the Promotion of Science (JSPS) KAKENHI Grant Number 15K21765, by a Grant-in-Aid for Young Scientists (A) (JP16H06030) from JSPS, by the Swiss National Science

Foundation, by the Swiss Nanoscience Institute, by COST action MP1303 'Understanding and Controlling nano and Mesoscale Friction'. P.S., J.T., and A.S.F. have been supported by the Academy of Finland through its Centres of Excellence Program Project No. 915804 and EU project PAMS (Contract No. 610446), and acknowledges use of the CSC, Helsinki for computational resources. We thank Juha Ritala for help in the development of the electrostatic model and particularly thank the referees for their efforts in improving the manuscript.

REFERENCES

- (1) Cava, M. P.; Mitchell, M. J. *Cyclobutadiene and Related Compounds*; Academic Press: New York, 1967.
- (2) Bally, T.; Masamune, S. *Cyclobutadiene. Tetrahedron* **1980**, *36*, 343–370.
- (3) Maier, G. *Tetrahedrane and Cyclobutadiene. Angew. Chem., Int. Ed. Engl.* **1988**, *27*, 309–332.
- (4) Inrgartinger, H.; Rodewald, H. The Structure of a Rectangular Cyclobutadiene. *Angew. Chem., Int. Ed. Engl.* **1974**, *13*, 740–741.
- (5) Delbaere, L. T. J.; James, M. N. G.; Nakamura, N.; Masamune, S. [4]Annulene System. Direct Proof for Its Rectangular Geometry. *J. Am. Chem. Soc.* **1975**, *97*, 1973–1974.
- (6) Inrgartinger, H.; Riegler, N.; Malsch, K.-D.; Schneider, K.-A.; Maier, G. Structure of Tetra-Tert-Butylcyclobutadiene. *Angew. Chem., Int. Ed. Engl.* **1980**, *19*, 211–212.
- (7) Deniz, A. A.; Peters, K. S.; Snyder, G. J. Experimental Determination of the Antiaromaticity of Cyclobutadiene. *Science* **1999**, *286*, 1119–1122.
- (8) Lothrop, W. C. Biphenylene. *J. Am. Chem. Soc.* **1941**, *63*, 1187–1191.
- (9) Hartman, A.; Hirshfeld, F. L. Structure of cis-1,2,3-Tricyanocyclopropane. *Acta Crystallogr.* **1966**, *20*, 80–82.
- (10) Jones, J. B.; Brown, D. S.; Hales, K. A.; Massey, A. G. Structure of Octamethylbiphenylene. *Acta Crystallogr., Sect. C: Cryst. Struct. Commun.* **1988**, *44*, 1757–1759.
- (11) Ferrara, J. D.; Solooki, D.; Tessier-Youngs, C.; Youngs, W. J. Structure of Benzo[b]biphenylene. *Acta Crystallogr., Sect. C: Cryst. Struct. Commun.* **1989**, *45*, 57–60.
- (12) Hine, J.; Ahn, K.; Gallucci, J. C.; Linden, S.-M. Structures of Double-Hydrogen-Bonded Adducts of 1,8-bi-Phenylenediol and Related Compounds. *Acta Crystallogr., Sect. C: Cryst. Struct. Commun.* **1990**, *46*, 2136–2146.
- (13) Yokozeki, A.; Wilcox, C. F., Jr; Bauer, S. H. Biphenylene. Internuclear Distances and Their Root Mean Square Amplitudes of Vibration. *J. Am. Chem. Soc.* **1974**, *96*, 1026–1032.
- (14) Ermer, O.; Heilbronner, E. Three Arguments Supporting a Rectangular Structure for Tetra-Tert-Butylcyclobutadiene. *Angew. Chem., Int. Ed. Engl.* **1983**, *22*, 402–403.
- (15) Inrgartinger, H.; Nixdorf, M. Bonding Electron Density Distribution in Tetra-Tert-Butylcyclobutadiene – A Molecule with an Obviously Non-Square Four-Membered Ring. *Angew. Chem., Int. Ed. Engl.* **1983**, *22*, 403–404.
- (16) Gross, L.; Mohn, F.; Moll, N.; Liljeroth, P.; Meyer, G. The Chemical Structure of a Molecule Resolved by Atomic Force Microscopy. *Science* **2009**, *325*, 1110–1114.
- (17) Gross, L.; Mohn, F.; Moll, N.; Meyer, G.; Ebel, R.; Abdel-Mageed, W. M.; Jaspars, M. Organic Structure Determination Using Atomic-Resolution Scanning Probe Microscopy. *Nat. Chem.* **2010**, *2*, 821–825.
- (18) Schuler, B.; Meyer, G.; Peña, D.; Mullins, O. C.; Gross, L. Unraveling the Molecular Structures of Asphaltenes by Atomic Force Microscopy. *J. Am. Chem. Soc.* **2015**, *137*, 9870–9876.
- (19) de Oteyza, D. G.; Gorman, P.; Chen, Y.-C.; Wickenburg, S.; Riss, A.; Mowbray, D. J.; Etkin, G.; Pedramrazi, Z.; Tsai, H.-Z.; Rubio, A.; Crommie, M. F.; Fischer, F. R. Direct Imaging of Covalent Bond Structure in Single-Molecule Chemical Reactions. *Science* **2013**, *340*, 1434–1437.
- (20) Kawai, S.; Haapasila, V.; Lindner, B. D.; Tahara, K.; Spijker, P.; Buitendijk, J. A.; Pawlak, R.; Meier, T.; Tobe, Y.; Foster, A. S.; Meyer, E. Thermal Control of Sequential On-Surface Transformation of a Hydrocarbon Molecule on a Copper Surface. *Nat. Commun.* **2016**, *7*, 12711.
- (21) Gross, L.; Mohn, F.; Moll, N.; Schuler, B.; Criado, A.; Guitián, E.; Peña, D.; Gourdon, A.; Meyer, G. Bond-Order Discrimination by Atomic Force Microscopy. *Science* **2012**, *337*, 1326–1329.
- (22) Pavliček, N.; Schuler, B.; Collazos, S.; Moll, N.; Pérez, D.; Guitián, E.; Meyer, G.; Peña, D.; Gross, L. On-surface Generation and Imaging of Arynes by Atomic Force Microscopy. *Nat. Chem.* **2015**, *7*, 623–628.
- (23) Pavliček, N.; Mistry, A.; Majzik, Z.; Moll, N.; Meyer, G.; Fox, D. J.; Gross, L. Synthesis and Characterization of Triangulene. *Nat. Nanotechnol.* **2017**, *12*, 308–311.
- (24) Schuler, B.; Fatayer, S.; Mohn, F.; Moll, N.; Pavliček, N.; Meyer, G.; Peña, D.; Gross, L. Reversible Bergman Cyclization by Atomic Manipulation. *Nat. Chem.* **2016**, *8*, 220–224.
- (25) Ward, E. R.; Pearson, B. D. The synthesis of 2:3–6:7-Dibenzodiphenylene, and a Note on the Reaction of 1-Bromo-2-Iodonaphthalene with Magnesium. *J. Chem. Soc.* **1959**, 1676–1680.
- (26) Ward, E. R.; Pearson, B. D. Reactions of Some Dihalogenonaphthalenes with Lithium Amalgam, and Simple Syntheses of 2,3,6,7-di-Benzobiphenylene. *J. Chem. Soc.* **1961**, 515–518.
- (27) Du Preez, N. P.; Van Vuuren, P. J.; Dekker, J. Synthetic Route to Dibenzo[b,h]biphenylene, and Its 5,6,11, and 12-Tetramethyl and -Tetraphenyl Derivatives. *J. Org. Chem.* **1970**, *35*, 523–527.
- (28) Wilcox, C. F.; Talwar, S. S. Two Syntheses of Dibenzo[b,h]biphenylene. *J. Chem. Soc. C* **1970**, 2162–2167.
- (29) Iyoda, M.; Kabir, S. H.; Vorasingha, A.; Kuwatani, Y.; Yoshida, M. Novel Synthesis of Biphenylene and Its Derivatives Using Intramolecular Coupling of Zinccyclopentadienes. *Tetrahedron Lett.* **1998**, *39*, 5393–5396.
- (30) Kabir, S. M. H.; Hasegawa, M.; Kuwatani, Y.; Yoshida, M.; Matsuyama, H.; Iyoda, M. Synthesis of Biphenylenes and Tetraphenylenes Using Copper-Catalyzed Coupling of Arylzinc Intermediates. *J. Chem. Soc., Perkin Trans.* **2001**, *1*, 159–165.
- (31) Kumar, B.; King, B. T. Synthesis of 1,8,9,16-Tetrakis(trimethylsilyl)tetra-cata-Tetrabenzoquadrannulene. *J. Org. Chem.* **2012**, *77*, 10617–10622.
- (32) Grill, L.; Dyer, M.; Lafferentz, L.; Persson, M.; Peters, M. V.; Hecht, S. Nano-Architectures by Covalent Assembly of Molecular Building Blocks. *Nat. Nanotechnol.* **2007**, *2*, 687–691.
- (33) Cai, J.; Ruffieux, P.; Jaafar, R.; Bieri, M.; Braun, T.; Blankenburg, S.; Muoth, M.; Seitsonen, A. P.; Saleh, M.; Feng, X.; Müllen, K.; Fasel, R. Atomically Precise Bottom-up Fabrication of Oraphene Nanoribbons. *Nature* **2010**, *466*, 470–473.
- (34) Kawai, S.; Saito, S.; Osumi, S.; Yamaguchi, S.; Foster, A. S.; Spijker, P.; Meyer, E. Atomically-Controlled Substitutional Boron-Doping of Graphene Nanoribbons. *Nat. Commun.* **2015**, *6*, 8098.
- (35) Björk, J.; Hanke, F.; Stafström, S. Mechanisms of Halogen-Based Covalent Self-Assembly on Metal Surfaces. *J. Am. Chem. Soc.* **2013**, *135*, 5768–5775.
- (36) Lipton-Duffin, J. A.; Ivasenko, O.; Perepichka, D. F.; Rosei, F. Synthesis of Polyphenylene Molecular Wires by Surface-Confined Polymerization. *Small* **2009**, *5*, 592–597.
- (37) Kawai, S.; Sadeghi, A.; Okamoto, T.; Mitsui, C.; Pawlak, R.; Takeya, J.; Goedecker, S.; Meyer, E. Organometallic Bonding in an Ullmann-Type On-Surface Chemical Reaction Studied by High-Resolution Atomic Force Microscopy. *Small* **2016**, *12*, 5303–5311.
- (38) Walch, H.; Gutzler, R.; Sirtl, T.; Eder, G.; Lackinger, M. Material- and Orientation-Dependent Reactivity for Heterogeneously Catalyzed Carbon-Bromine Bond Homolysis. *J. Phys. Chem. C* **2010**, *114*, 12604–12608.
- (39) Eichhorn, J.; Strunskus, T.; Rastgoo-Lahrood, A.; Samanta, D.; Schmittele, M.; Lackinger, M. On-Surface Ullmann polymerization via Intermediate Organometallic Networks on Ag(111). *Chem. Commun.* **2014**, *50*, 7680–7682.

- (40) Curtis, R. F.; Viswanath, G. The Synthesis of 2:3–6:7-Dibenzodiphenylene. *J. Chem. Soc.* **1959**, 1670.
- (41) Weymouth, A. J.; Hofmann, T.; Giessibl, F. J. Quantifying Molecular Stiffness and Interaction with Lateral Force Microscopy. *Science* **2014**, *343*, 1120–1122.
- (42) Schuler, B.; Liu, W.; Tkatchenko, A.; Moll, N.; Meyer, G.; Mistry, A.; Fox, D.; Gross, L. Adsorption Geometry Determination of Single Molecules by Atomic Force Microscopy. *Phys. Rev. Lett.* **2013**, *111*, 106103.
- (43) Sader, J. E.; Jarvis, S. P. Accurate Formulas for Interaction Force and Energy in Frequency Modulation Force Spectroscopy. *Appl. Phys. Lett.* **2004**, *84*, 1801.
- (44) Rampulla, D. M.; Gellman, A. J.; Sholl, D. S. Bromine Atom Diffusion on Stepped and Kinked Copper Surfaces. *Surf. Sci.* **2006**, *600*, 2171–2177.
- (45) Pauling, L. Atomic Radii and Interatomic Distances in Metals. *J. Am. Chem. Soc.* **1947**, *69*, 542–553.
- (46) Giessibl, F. J. High-Speed Force Sensor for Force Microscopy and Profilometry Utilizing a Quartz Tuning Fork. *Appl. Phys. Lett.* **1998**, *73*, 3956–3958.
- (47) Giessibl, F. J. Advances in Atomic Force Microscopy. *Rev. Mod. Phys.* **2003**, *75*, 949–983.
- (48) Albrecht, T. R.; Grütter, P.; Horne, D.; Rugar, D. Frequency Modulation Detection Using High-Q Cantilevers for Enhanced Force Microscope Sensitivity. *J. Appl. Phys.* **1991**, *69*, 668–673.
- (49) Bartels, L.; Meyer, G.; Rieder, K.-H. Controlled Vertical Manipulation of Single CO Molecules with the Scanning Tunneling Microscope: A Route to Chemical Contrast. *Appl. Phys. Lett.* **1997**, *71*, 213–215.
- (50) Horcas, I.; Fernandez, R.; Gomez-Rodriguez, J.; Colchero, J.; Gomez-Herrero, J.; Baro, A. WSXM: A Software for Scanning Probe Microscopy and a Tool for Nanotechnology. *Rev. Sci. Instrum.* **2007**, *78*, 013705.
- (51) Kresse, G.; Furthmüller, J. Efficiency of *ab-initio* Total Energy Calculations for Metals and Semiconductors Using a Plane-Wave Basis Set. *Comput. Mater. Sci.* **1996**, *6*, 15–50.
- (52) Kresse, G.; Furthmüller, J. Efficient Iterative Schemes for *ab initio* Total-Energy Calculations Using a Plane-Wave Basis Set. *Phys. Rev. B: Condens. Matter Mater. Phys.* **1996**, *54*, 11169–11186.
- (53) Klimeš, J.; Bowler, D. R.; Michaelides, A. Chemical Accuracy for the van der Waals Density Functional. *J. Phys.: Condens. Matter* **2010**, *22*, 022201.
- (54) Klimeš, J.; Bowler, D. R.; Michaelides, A. Van der Waals Density Functionals Applied to Solids. *Phys. Rev. B: Condens. Matter Mater. Phys.* **2011**, *83*, 195131.
- (55) Björkman, T.; Gulans, A.; Krashennnikov, A. V.; Nieminen, R. M. van der Waals Bonding in Layered Compounds from Advanced Density-Functional First-Principles Calculations. *Phys. Rev. Lett.* **2012**, *108*, 235502.
- (56) Blöchl, P. E. Projector Augmented-Wave Method. *Phys. Rev. B: Condens. Matter Mater. Phys.* **1994**, *50*, 17953.
- (57) Tang, W.; Sanville, E.; Henkelman, G. A Grid-Based Bader Analysis Algorithm without Lattice Bias. *J. Phys.: Condens. Matter* **2009**, *21*, 084204.
- (58) Becke, A. D. Density-Functional Thermochemistry. III. The Role of Exact Exchange. *J. Chem. Phys.* **1993**, *98*, 5648–5652.
- (59) Stephens, P. J.; Devlin, F. J.; Chabalowski, C. F.; Frisch, M. J. *Ab Initio* Calculation of Vibrational Absorption and Circular Dichroism Spectra Using Density Functional Force Fields. *J. Phys. Chem.* **1994**, *98*, 11623–11627.
- (60) Grimme, S.; Antony, J.; Ehrlich, S.; Krieg, H. A Consistent and Accurate *ab initio* Parametrization of Density Functional Dispersion Correction (DFT-D) for the 94 Elements H-Pu. *J. Chem. Phys.* **2010**, *132*, 154104.
- (61) Tkatchenko, A.; Scheffler, M. Accurate Molecular Van Der Waals Interactions from Ground-State Electron Density and Free-Atom Reference Data. *Phys. Rev. Lett.* **2009**, *102*, 073005.
- (62) Hapala, P.; Kichin, G.; Wagner, C.; Tautz, F. S.; Temirov, R.; Jelínek, P. Mechanism of High-Resolution STM/AFM Imaging with Functionalized Tips. *Phys. Rev. B: Condens. Matter Mater. Phys.* **2014**, *90*, 085421.
- (63) Hapala, P.; Temirov, R.; Tautz, F. S.; Jelínek, P. Origin of High-Resolution IETS-STM Images of Organic Molecules with Functionalized Tips. *Phys. Rev. Lett.* **2014**, *113*, 226101.
- (64) Hapala, P.; Svec, M.; Stetsovych, O.; van der Heijden, N. J.; Ondráček, M.; van der Lit, J.; Mutombo, P.; Swart, I.; Jelínek, P. Mapping the Electrostatic Force Field of Single Molecules from High-Resolution Scanning Probe Images. *Nat. Commun.* **2016**, *7*, 11560.